NASA/TM—2010-216804

Hypervelocity Impact of Unstressed and Stressed Titanium in a Whipple Configuration in Support of the Orion Crew Exploration Vehicle Service Module Propellant Tanks

Henry K. Nahra
Glenn Research Center, Cleveland, Ohio

Eric Christiansen
Johnson Space Center, Houston, Texas

Andrew Piekutowski
University of Dayton Research Institute, Dayton, Ohio

Frankel Lyons
Johnson Space Center, Houston, Texas

Christopher Keddy
White Sands Test Facility, Las Cruces, New Mexico

Jonathan Salem
Glenn Research Center, Cleveland, Ohio

Joshua Miller and William Bohl
Lockheed Martin, Space Systems Company, Denver, Colorado

Kevin Poormon
University of Dayton Research Institute, Dayton, Ohio

Nathanael Greene and Karen Rodriguez
White Sands Test Facility, Las Cruces, New Mexico

October 2010

NASA STI Program . . . in Profile

Since its founding, NASA has been dedicated to the advancement of aeronautics and space science. The NASA Scientific and Technical Information (STI) program plays a key part in helping NASA maintain this important role.

The NASA STI Program operates under the auspices of the Agency Chief Information Officer. It collects, organizes, provides for archiving, and disseminates NASA's STI. The NASA STI program provides access to the NASA Aeronautics and Space Database and its public interface, the NASA Technical Reports Server, thus providing one of the largest collections of aeronautical and space science STI in the world. Results are published in both non-NASA channels and by NASA in the NASA STI Report Series, which includes the following report types:

- TECHNICAL PUBLICATION. Reports of completed research or a major significant phase of research that present the results of NASA programs and include extensive data or theoretical analysis. Includes compilations of significant scientific and technical data and information deemed to be of continuing reference value. NASA counterpart of peer-reviewed formal professional papers but has less stringent limitations on manuscript length and extent of graphic presentations.

- TECHNICAL MEMORANDUM. Scientific and technical findings that are preliminary or of specialized interest, e.g., quick release reports, working papers, and bibliographies that contain minimal annotation. Does not contain extensive analysis.

- CONTRACTOR REPORT. Scientific and technical findings by NASA-sponsored contractors and grantees.

- CONFERENCE PUBLICATION. Collected papers from scientific and technical conferences, symposia, seminars, or other meetings sponsored or cosponsored by NASA.

- SPECIAL PUBLICATION. Scientific, technical, or historical information from NASA programs, projects, and missions, often concerned with subjects having substantial public interest.

- TECHNICAL TRANSLATION. English-language translations of foreign scientific and technical material pertinent to NASA's mission.

Specialized services also include creating custom thesauri, building customized databases, organizing and publishing research results.

For more information about the NASA STI program, see the following:

- Access the NASA STI program home page at *http://www.sti.nasa.gov*

- E-mail your question via the Internet to *help@sti.nasa.gov*

- Fax your question to the NASA STI Help Desk at 443–757–5803

- Telephone the NASA STI Help Desk at 443–757–5802

- Write to:
  NASA Center for AeroSpace Information (CASI)
  7115 Standard Drive
  Hanover, MD 21076–1320

NASA/TM—2010-216804

Hypervelocity Impact of Unstressed and Stressed Titanium in a Whipple Configuration in Support of the Orion Crew Exploration Vehicle Service Module Propellant Tanks

Henry K. Nahra
Glenn Research Center, Cleveland, Ohio

Eric Christiansen
Johnson Space Center, Houston, Texas

Andrew Piekutowski
University of Dayton Research Institute, Dayton, Ohio

Frankel Lyons
Johnson Space Center, Houston, Texas

Christopher Keddy
White Sands Test Facility, Las Cruces, New Mexico

Jonathan Salem
Glenn Research Center, Cleveland, Ohio

Joshua Miller and William Bohl
Lockheed Martin, Space Systems Company, Denver, Colorado

Kevin Poormon
University of Dayton Research Institute, Dayton, Ohio

Nathanael Greene and Karen Rodriguez
White Sands Test Facility, Las Cruces, New Mexico

Prepared for the
11th Hypervelocity Impact Symposium 2010
sponsored by the Hypervelocity Impact Society
Freiburg, Germany, April 11–15, 2010

National Aeronautics and
Space Administration

Glenn Research Center
Cleveland, Ohio 44135

October 2010

Acknowledgments

The authors wish to thank the National Aeronautics and Space Administration and the Orion program for funding this effort.

Level of Review: This material has been technically reviewed by technical management.

Available from

NASA Center for Aerospace Information
7115 Standard Drive
Hanover, MD 21076–1320

National Technical Information Service
5301 Shawnee Road
Alexandria, VA 22312

Available electronically at http://gltrs.grc.nasa.gov

Hypervelocity Impact of Unstressed and Stressed Titanium in a Whipple Configuration in Support of the Orion Crew Exploration Vehicle Service Module Propellant Tanks

Henry K. Nahra
National Aeronautics and Space Administration
Glenn Research Center
Cleveland, Ohio 44135

Eric Christiansen
National Aeronautics and Space Administration
Johnson Space Center
Houston, Texas 77058

Andrew Piekutowski
University of Dayton Research Institute
Dayton, Ohio 45469

Frankel Lyons
National Aeronautics and Space Administration
Johnson Space Center
Houston, Texas 77058

Christopher Keddy
White Sands Test Facility
Las Cruces, New Mexico 88004

Jonathan Salem
National Aeronautics and Space Administration
Glenn Research Center
Cleveland, Ohio 44135

Joshua Miller and William Bohl
Lockheed Martin Space Systems Company
Denver, Colorado 80201

Kevin Poormon
University of Dayton Research Institute
Dayton, Ohio 45469

Nathanael Greene and Karen Rodriguez
White Sands Test Facility
Las Cruces, New Mexico 88004

Abstract

Hypervelocity impacts were performed on six unstressed and six stressed titanium coupons with aluminum shielding in order to assess the effects of the partial penetration damage on the post impact micromechanical properties of titanium and on the residual strength after impact. This work is performed in support of the definition of the penetration criteria of the propellant tanks' surfaces for the service module of the crew exploration vehicle where such a criterion is based on testing and analyses rather than on historical precedence. The objective of this work is to assess the effects of applied biaxial stress on the damage dynamics and morphology. The crater statistics revealed minute differences between stressed and unstressed coupon damage. The post impact residual stress analyses showed that the titanium strength properties were generally unchanged for the unstressed coupons when compared with undamaged titanium. However, high localized strains were shown near the craters during the tensile tests.

Nomenclature

C	Speed of sound in materials, km/s
d_p	Projectile diameter, cm, mm
E	Young's modulus, ksi, MPa
H	Brinell hardness
HV	Vickers Hardness
P_∞	Crater depth, cm
t_b	Bumper thickness, cm
V_{fragment}	Fragment velocity, km/s
V_p	Projectile velocity, km/s
$\in_{xx}$	Strain along x direction, percent
$\in_{yy}$	Strain along y direction, percent
σ_{xx}	Normal Stress Component along x direction, ksi, MPa
σ_{yy}	Normal Stress Component along y direction, ksi, MPa
ν	Poisson Ratio
ρ_p	Projectile density, g/cm^3
ρ_t	Target density, g/cm^3

1.0 Introduction

The propellant tanks on the service module of the Orion Crew Exploration Vehicle (CEV) are vulnerable to the micrometeoroids and orbital debris (MMOD) impacts. Although they are shielded by other surfaces, a projectile of significant energy could penetrate through the shielding. Generated fragmentation could impact the surfaces of the propellant tanks and result in adverse effects on the service module. The spectrum of damage ranges from a perforation through the tank wall to simple cratering of the surfaces of the tanks. The allowable depth of penetration in the surface of the propellant tank is integral to the definition of the failure criteria used in the MMOD system level analysis of the vehicle. The current allowable penetration criteria for the pressure vessels on board of the Service Module (SM) of the CEV are based on historical background; however, these criteria should be based on experiments and analyses that show that the allowable depth of penetration is reasonable and not overly conservative or nonconservative.

An experimental program aimed at addressing the depth of penetration that is allowed on the tanks surfaces with multicenter and multidisciplinary participation was planned in support of NASA's future missions. Phase 1 of the program addresses the penetration depth of metallic titanium tank surfaces whereas phase 2 addresses the penetration depth into the composite surface of composite overwrapped pressure vessels (COPV). A building block approach is adopted in this program. For phase 1, which is

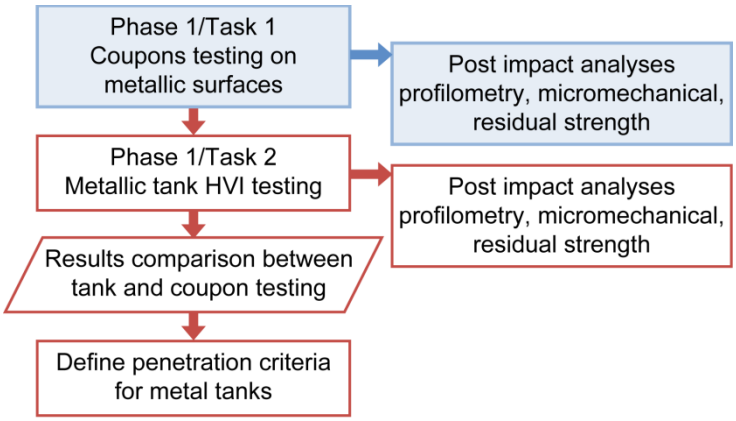

Figure 1.—Block diagram of phase 1 with the presented work highlighted in blue.

concerned with the titanium surface, six stressed and unstressed titanium coupons shielded with aluminum bumpers were hypervelocity impacted by projectiles that penetrate the aluminum shield and cause the resulting plume to impact the titanium surface to produce a partial penetration distribution of craters. A series of post impact analyses are performed to assess the damage resulting from the craters. Detailed comparisons are performed to assess the difference between biaxially loaded and unstressed coupons impacted with similar projectiles and nearly similar velocities. Testing of pressurized titanium metal tanks is planned through task 2 of phase 1. This paper is focused on the hypervelocity impact (HVI) testing of the titanium coupons and the craters analyses that followed. Figure 1 shows a basic block diagram for phase 1 effort with the presented work highlighted in blue.

2.0 Testing

In this effort, the conducted HVI experiments consisted of performing six shots on aluminum-shielded unstressed titanium coupons at White Sands Test Facility (WSTF), and six shots on aluminum-shielded-biaxially-stressed titanium coupons at the University of Dayton Research Institute (UDRI)-Impact Physics Laboratories. The configurations of the test coupons were similar except for the biaxial stress state.

2.1 Target-Shielding Geometry

Figure 2(a) shows a schematic of the coupon geometry. The basic configuration of the test article consisted of a 0.0965 cm (0.04 in.) aluminum 6061-T6 bumper and a 0.127 cm (0.05 in.) Titanium (Ti-6Al-4V) substrate with a standoff distance of 27.9 cm (11 in.). Similar configuration for the unstressed coupons was adopted. Although this geometry and configuration does not fully reflect the shielding design of the service module tanks, this configuration was chosen for the fact that it makes the crater analysis much more correlated with the projectile speed, density and velocity because the Whipple shield is well understood from a fundamental stand point. No material backing of the titanium was considered because we decided to pursue the worst case where the tank wall is contacting the gas and where the greatest mismatch in mechanical impedance occurs.

2.2 Biaxial Stress Fixture

A biaxial stress fixture was designed and fabricated at UDRI for this series of testing. It was based on the design of the uniaxial stress fixture used for the crack propagation studies of the International Space Station (ISS) module skin. The biaxial fixture is shown in Figure 2(b). This fixture is capable of providing

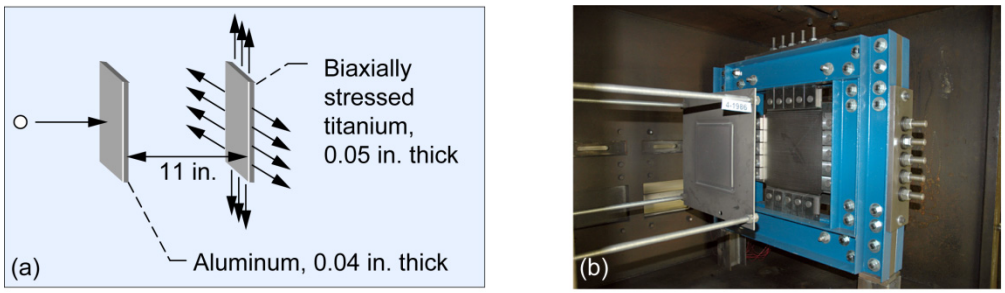

Figure 2.—(a) Schematic of the experimental setup of the stressed Ti coupons and (b) shows the biaxial stress fixture with the titanium coupon installed.

TABLE 1.—HVI TESTS ON UNSTRESSED AND STRESSED Ti COUPONS WITH ALUMINUM SHIELDS

WSTF/HITF Number	*UDRI Test #*	*Projectile Type*	*Projectile Diameter (mm)*	*Requested Velocity (km/s)*	*Impact Angle (deg)*	*Estimated Penetration of 1.27 mm Ti mm-(%)*
HITF08373	#1	Al 2017-T4	1.6	7.0	0	0.165-13%
HITF08374	#2	Al 2017-T4	2.0	7.0	0	0.24 - 19%
HITF08375	#3	Al 2017-T4	2.6	7.0	0	0.37-29%
HITF08376	#4	Nylon	2.0	7.0	0	0.14-11%
HITF08377	#5	Nylon	3.6	7.0	0	0.34-27%
HITF08378	#6	Al 2017-T4	3.6	7.0	0	0.53-42%

80 ksi±7 percent of biaxial stress which was a requirement reflecting the stress state of typical metallic propellant tanks. The calibration of the biaxial stress state was performed with eight biaxial strain gages (4 gauges in each direction). Five turnbuckles along the vertical and horizontal direction provided the mechanical pull to achieve the calibrated strain that corresponds to the desired stress level. The titanium coupons were first installed in the fixture. Before performing the hypervelocity impact, the titanium was strained to the appropriate strain level of 3248 μ *strains* in each direction based on the aforementioned biaxial stress of 80 ksi. The strain level was computed from the two-dimensional Hooke's law given by,

$$\varepsilon_{xx} = \frac{1}{E}\left(\sigma_{xx} - \nu\sigma_{yy}\right); \quad \varepsilon_{yy} = \frac{1}{E}\left(\sigma_{yy} - \nu\sigma_{xx}\right) \tag{1}$$

Where σ_{xx} is the normal stress component along the x direction, ε_{xx} is the strain along the *x* direction, E is Young's Modulus, and ν is the Poisson ratio. The strain along the vertical direction is computed from the ε_{yy} equation also given in Equation (1).

The titanium coupons for the unstressed tests were integrated with the aluminum shielding according to the spacing given in paragraph 2.1. For the stressed coupons, the configuration differed a little in that the titanium could not be integrated with the aluminum shielding. Instead, the aluminum shield was installed on a different structure as shown in Figure 1(b) and titanium target was installed into the biaxial stress fixture. The titanium thickness was milled down to 0.127 cm (0.05 in.) in an area in the middle of the coupon of 22.9 by 22.9 cm (9 by 9 in.).

2.3 Test Matrices for the Unstressed and Stressed Coupons Tests

The test plan matrix for the unstressed and stressed titanium coupons is shown in Table 1, respectively. The first and second columns refer to the reference numbers of the tests performed at WSTF (unstressed) and UDRI (biaxially stressed), respectively. The Whipple shield Ballistic Limit Equation (BLE) was used to estimate the depth of penetration shown in the last column of the table.

In general, the parameters were made very similar for comparison purposes in order to look for the effects of the biaxial stress on the micro-mechanical features of the craters and the residual strength of the titanium. The aluminum projectiles simulate the orbital debris environment whereas the micrometeoroids are simulated with the lower density nylon projectiles. The higher micrometeoroids velocity is not simulated because of the limitations of the launch facilities used for the hypervelocity impacts.

3.0 Results

The results for the unstressed and stressed titanium coupons HVIs will be presented in this section of the paper and these encompassed several post impact analyses performed on the craters.

3.1 Crater Depth Analyses

Several craters in each of the impacted coupons were analyzed for depth and diameter. The craters were chosen based on their visual appearance as being of greater depth and diameter. The depth of penetration for each of the crater was measured with the three-dimensional microscope at the Johnson Space Center. A typical depth image and profile is shown in Figure 3. The craters were identified by placing and lining up a transparency over the titanium coupon and identifying with a marker the craters of interest. Then the transparency which served as a reference catalog was removed to look at the chosen craters. Table 2 shows the results of analyzing 5 craters on an unstressed titanium coupon where the projectile diameter was 1.6 mm at 6.69 km/s.

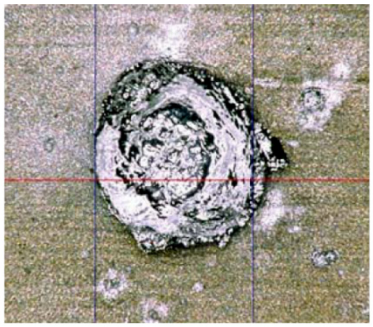

Figure 3.—Three-dimensional microscope image of a crater of 0.545- by 0.619-mm and 147.6 μm of depth equivalent to 12 percent depth of penetration.

TABLE 2.—DEPTH OF PENETRATION FOR THE 5 CRATERS MEASURED ON THE TITANIUM COUPON FROM A 1.6 mm ALUMINUM PROJECTILE IMPACT ON ALUMINUM

Crater ID	*Ti-6Al-4V Rear Wall Crater Damage*	*Penetration %*
HITF08373-5	0.545 mmx0.619mmx147.6μm deep	11.6
HITF08373-14	0.768mmx.676mmx175.7μm deep	13.8
HITF08373-19	0.537mmx0.847mmx203.8μm deep	16
HITF08373-20	0.695mmx0.684mmx102.6μm deep	8.1
HITF08373-21	0.716mmx0.472mmx164.5μm deep	13

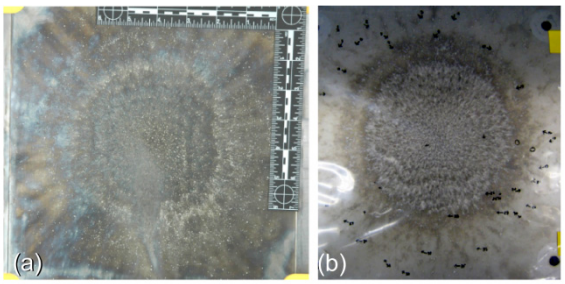

Figure 4.—Secondary plume impact on stressed (a) and unstressed (b) Titanium for a 2.6-mm aluminum projectile at 6.96 and 7.32 km/s, respectively.

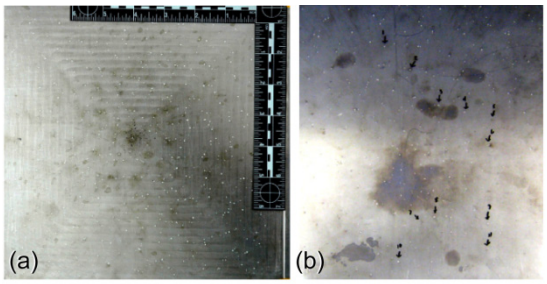

Figure 5.—Secondary plume impact on stressed (a) and unstressed (b) Titanium for a 3.6-mm nylon projectile at 7 and 6.87 km/s.

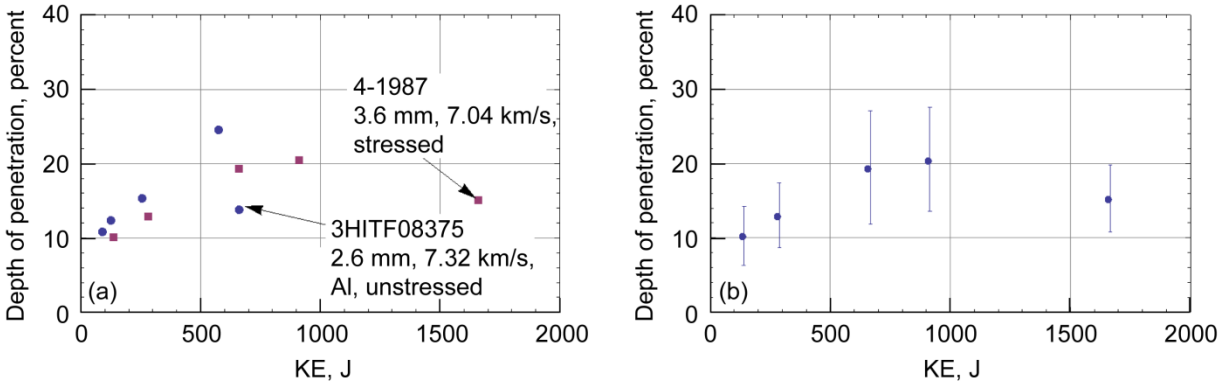

Figure 6.—(a) Depth of penetration as a function of the projectile kinetic energy. Blue circles (red squares) correspond to the unstressed coupons (stressed coupons). (b) 95 percent confidence interval depth of penetration as a function of the projectile kinetic energy for the stressed Ti coupon.

Figure 4(a) and (b) shows the damage distribution on a stressed and unstressed titanium surface from a 2.6 mm projectile that impacted the aluminum shield. It is observed that the ring structure is apparent for the aluminum projectile but not so apparent for the 3.6 mm nylon projectile shown in Figure 5(a) and (b).

Moreover, there seems to be no dependence of the crater depth on the radial distance from the impact center for both the stressed and unstressed coupons and for the aluminum and nylon projectiles. The titanium coupons impacted with plumes from aluminum projectile-aluminum shield showed concentric ring structures that are reflective of the projectile diameter and the plume generated from the projectile impact with the aluminum surface. Although the ring structure exists, the lack of dependence of the crater depth on the radial distance from the center suggests that the craters were generated by aluminum particles released from the aluminum bumper and landed on the outskirts of the aforementioned rings of particle damage.

As shown in Figures 4 and 5, secondary impacts resulted in similar damage maps on the stressed and unstressed coupons for the aluminum and nylon projectiles, respectively. The nylon density is almost three times less than the aluminum density with a lower melting and vaporization temperatures. With similar impact loading pressure on the aluminum, the nylon projectile vaporizes and the resulting plume is primarily made up of particles released from the aluminum shield. These particles are on the average greater in size than those released from impacts of aluminum projectiles on the aluminum shield.

In the crater analyses performed at the NASA Johnson Space Center, the crater depth and diameter were measured at selected damage sites. The average damage depth for each of the titanium coupons was calculated from the various craters. Figure 6 shows the crater depth plotted as a function of the projectile kinetic energy for the stressed and unstressed coupons with the 95 percent confidence interval calculated for the stressed coupons' measured craters shown in Figure 6(b). The decreasing trend at higher projectile kinetic energy may be explained by the smaller particles in the plume generated by the higher loading impact pressure from the bigger aluminum projectiles.

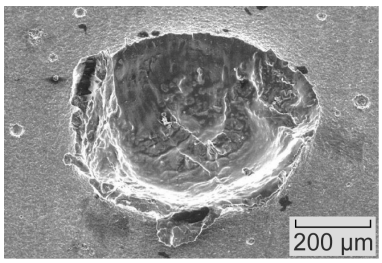

Figure 7.—SEM of a crater from a particle in a plume resulting from 1.6-mm aluminum projectile. The crater's depth is 11.6 percent of thickness.

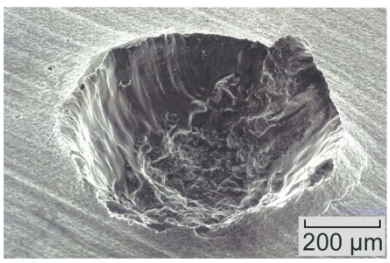

Figure 8.—Shows an SEM of a crater from a particle in a plume resulting from 2.6-mm aluminum projectile. The crater's depth is 25.4 percent of thickness.

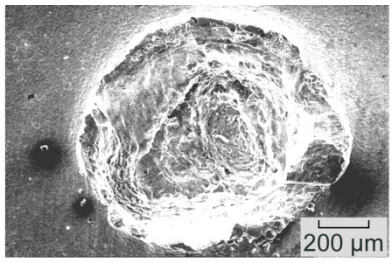

Figure 9.—Shows an SEM of a crater from a particle in a plume resulting from 2.0-mm aluminum projectile. The crater's depth is 38 percent of thickness.

3.2 Micromechanical-Metallographic Analyses

The micromechanical analyses performed at WSTF focused on assessing the micromechanical properties of the titanium near selected craters of specific penetration depths. Three craters were chosen from three titanium coupons. Two craters came from the titanium coupons of tests HITF08373 and HITF08375, respectively whereas the third from the titanium coupon of HITF08377. These three craters were chosen on the titanium coupons and a small sample was cut around each of the craters. The craters' depths were about 12, 25, and 38 percent of the titanium thickness.

3.2.1 Scanning Electron Microscopy

At first, scanning electron microscopy (SEM) was performed on the three samples to obtain a crater profile and determine an accurate depth of the crater. Figures 7 and 8 show SEM images of the craters from the 1.6 and 2.6 mm aluminum projectile whereas Figure 9 shows an image of the crater that resulted from the nylon impact on the aluminum bumper.

3.2.2 Replica Metrology and White Light Profilometry

In an effort to assess the effectiveness of making a replica for the damage which in turn will be used for white light profilometry, replica metrology was performed on the craters utilizing a polymeric rubbery system. The replicas were allowed to cure and detached from the target plate on both the crater side as well as the back side in the region situated just below the crater. White light profilometry was performed on the single craters as well as on the plate surface just behind the crater prior to sectioning. As shown in Figure 10, there is a close correspondence (a difference of 10 percent) between the replica and the crater obtained from the 1.6 mm aluminum projectile impact on the aluminum shield, and the results were consistent between the profiles acquired from the crater and the replicas.

3.2.3 Metallography

Once white light profilometry was completed, the craters were sectioned in the transverse orientation and the sectioned half crater was cold mounted and polished utilizing standard metallographic techniques. Once the mounted samples had been polished to approximately the middle of the crater, a Kroll's reagent was used to etch it. As shown in Figures 11 and 12, the micrographs revealed equiaxed α with intergranular β as would be expected for an annealed Ti-6Al-4V. Several spall cracks were observed (Fig. 12) on both sides of the sectioned crater for only the nylon impactor. The back side of the target plate just below the crater was also imaged and no spall cracks were observed. A direct comparison of the damage range for the nylon projectiles for both the stressed and unstressed Ti coupons shows that the maximum damage measured for the finite number of samples tends to be about 40 percent. Such deep depth of penetration presents concerns since it is shown later that the scanning electron micrographs of such deep impact exhibited spall microcracks near the crater.

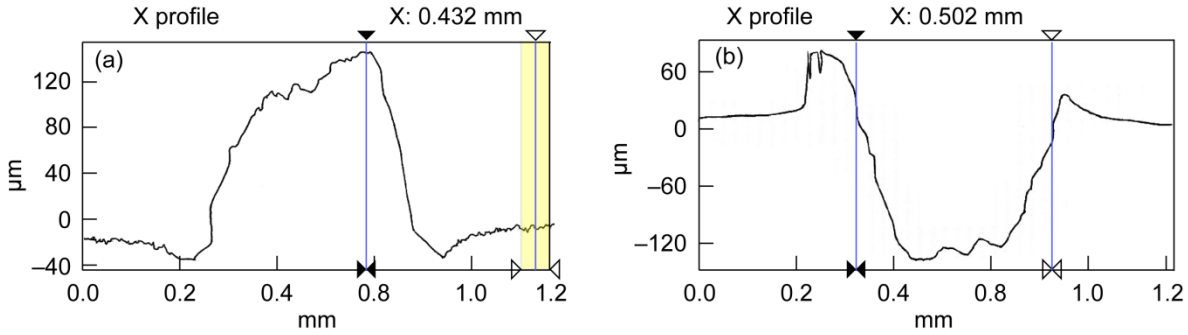

Figure 10.—White light profilometry scan for the replica (a) and the crater (b) for the x profile.

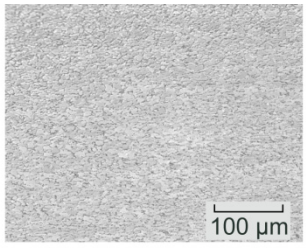

Figure 11.—Equiaxed α and intergranual β phases in the annealed Ti-6Al-4V alloy.

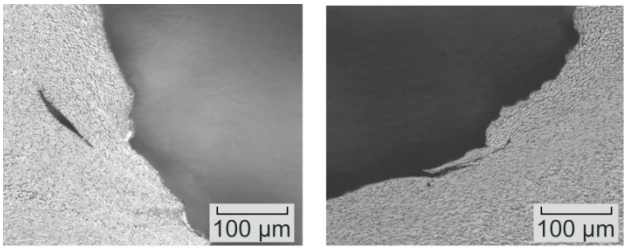

Figure 12.—Shows two spall cracks on both sides of the sectioned crater for a nylon impactor.

3.2.4 Vickers Hardness—Unstressed Titanium Coupons

Hardness was measured on the sectioned and mounted crater utilizing a Vickers micro-hardness tester with a 100 g load. Hardness readings were taken on the base metal as well as from the base of the crater all the way to the back face of the target plate as shown in Figure 13. Figure 14 shows a summary of the measured Vickers micro-hardness as a function of the distance below the crater for the three craters that were sectioned.

The micro-hardness profile below the crater does not appear to show a very significant hardness change in the base metal as a result of the impact. For instance for the nylon projectile related crater, Vickers micro-hardness ranged from 285 to 326 HV whereas the base material hardness was found to be in the range of 300 to 350 HV with the highest reading located just below the front target plate face.

3.2.5 Energy Dispersive X-Ray Spectroscopy

Energy-dispersive x-ray spectroscopic (EDS) analysis was performed on control titanium samples as well as on the inside of the crater. The EDS technique is capable of detecting elements of atomic number 4 (Beryllium) and greater. As shown in Figure 15(b), the inside of the crater possessed an intense aluminum peak which most likely is the result of deposition of the projectile (2017-T4 aluminum) or bumper plate material (6061-T6 aluminum) on the crater inner wall.

3.3 Bumper Fragments Size Estimates

An attempt was made to calculate the particle distribution for each of the impacts on the unstressed and shielded titanium coupons. Based on the ratio of the bumper thickness to the impacting projectile diameter t_b/d_p which ranged between 0.2 to 0.6, and on the projectile velocity being about 7 km/s, the projectile may have been partially or fully melted upon impact but the bumper unlike the projectile is fragmented and the fragments partially penetrated the titanium surface (Ref. 1). The craters produced from the aluminum projectile impacts and that were chosen for depth measurements lied on the outskirt of the ring structures that formed on the titanium. These craters were created by aluminum fragments that were broken off from the bumper. The nylon projectile most likely vaporizes upon impact and consequently, the craters are also formed from the aluminum fragments that are broken from the shield.

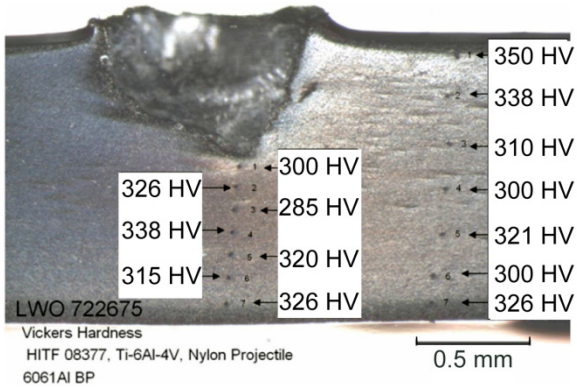

Figure 13.—Shows the Vickers hardness measurements of the surface below the crater related to the nylon projectile on aluminum bumper.

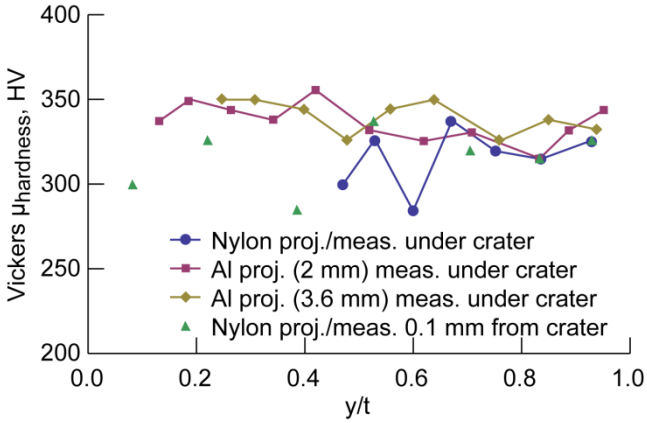

Figure 14.—Summary of the Vickers hardness date plotted as a function of ratio y/t of the distance from the bottom of the crater (y) to the titanium sheet thickness (t).

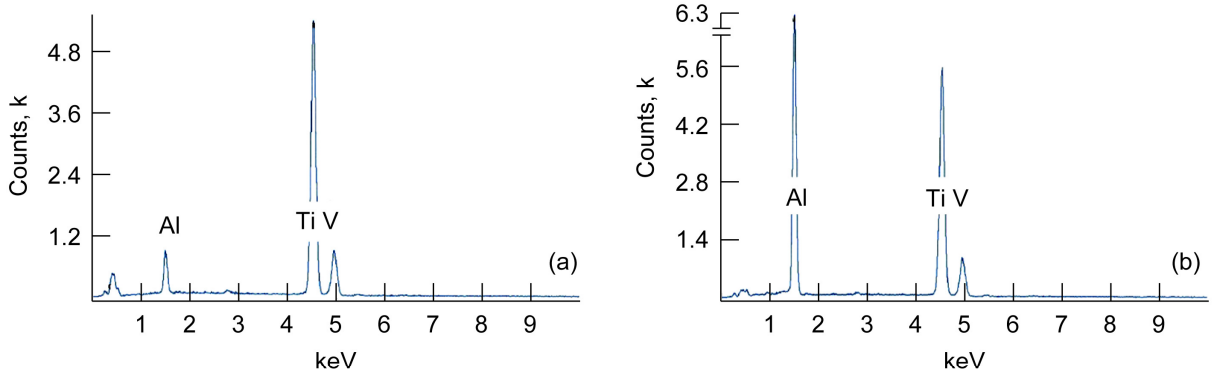

Figure 15.—EDS spectra for titanium plate material (a) and for inside of the crater (b). It is worth noting that the first peak in (b) is attributed to aluminum from the projectile or the bumper and that the NIST traceable SRM has extremely close signature to the titanium plate.

The crater depth information was used to approximate the diameter or the length scale of the impacting fragments. This was done using the penetration depth equation and back calculating the impacting diameter. The penetration depth that results from an impacting particle of diameter d_p and a velocity V_p is given for $\rho_p/\rho_t < 1.5$ by (Ref. 2),

$$P_\infty = \frac{5.24 d_p^{19/18}}{\sqrt[4]{H}} \sqrt{\left(\frac{\rho_p}{\rho_t}\right)} \left(\frac{V_p}{C}\right)^{2/3} \tag{2}$$

P_∞ is the depth in a semi-infinite target, H is the Brinell hardness, ρ_p and ρ_t are the projectile and target densities respectively, and C is the speed of sound in the material interacting with the projectile. The maximum fragment diameter from the aluminum bumper cannot exceed the bumper thickness. The velocity of the bumper fragments is related to the impact velocity by (Ref. 2),

$$V_{\text{fragments}} = 0.8 V_p e^{-t_b/d_p} \tag{3}$$

Combination of Equations (2) and (3), realizing that d_p in Equation (2) is actually d_{fragment}, and solving for d_{fragment} leads to,

$$d_{\text{fragment}} = \left(\frac{P_\infty \sqrt[4]{H}}{5.24 \sqrt{\left(\rho_p/\rho_t\right)} \left(V_{\text{fragment}}/C\right)^{2/3}} \right)^{18/19} \tag{4}$$

The distribution of the fragment diameter/length scale based on the depth of the few craters from the unstressed (Fig. 6(a), (c), and (e)) and stressed (Fig. 6(b), (d), and (f)) coupons that were measured is shown in Figure 16(a) to (f). In Figure 16(e) and (f), the distribution of all particles from all the impacts performed on the unstressed and stressed coupons is shown, respectively. The range of the particles length scale is comparable for the stressed and unstressed titanium and for the different projectile diameters. The fragmentation distribution depends on the bumper properties and the projectile energy. The titanium cratering was used to gage the plume distribution. Figure 16(e) and (f) suggest that the fragmentation distribution from the shield ranged in size from 0.02 to about 0.1 cm. The majority of the fragmentation size is between 0.02 and 0.04 cm in diameter for the aluminum projectiles ranging from 1.6 to 3.6 mm and nylon projectiles from 2 mm to about 3.6 mm.

3.4 Residual Strength Measurements

The residual strength measurements were performed at the NASA Glenn Research Center. The tensile strength of the unstressed cratered titanium sheets was performed by using ASTM E8 (Ref. 3) sub-sized specimens cut from the impact site. The 1 in. gage section of the test specimens was centered on regions exhibiting multiple, large craters or significant debris splatter. Prior to testing, the depth, width, and length of the largest craters in each gage section were measured. The largest craters were ~1.1 by 1.0 by 0.5 mm in width, length, and depth, respectively. For the specimens exhibiting the worst apparent damage (i.e., largest craters), the strain field in the gage section was recorded during loading by using a camera-based displacement system. This allowed estimation of the local stress/strain concentration around the crater.

The engineering tensile properties of reference (undamaged) and cratered titanium sheets are given in Table 3.

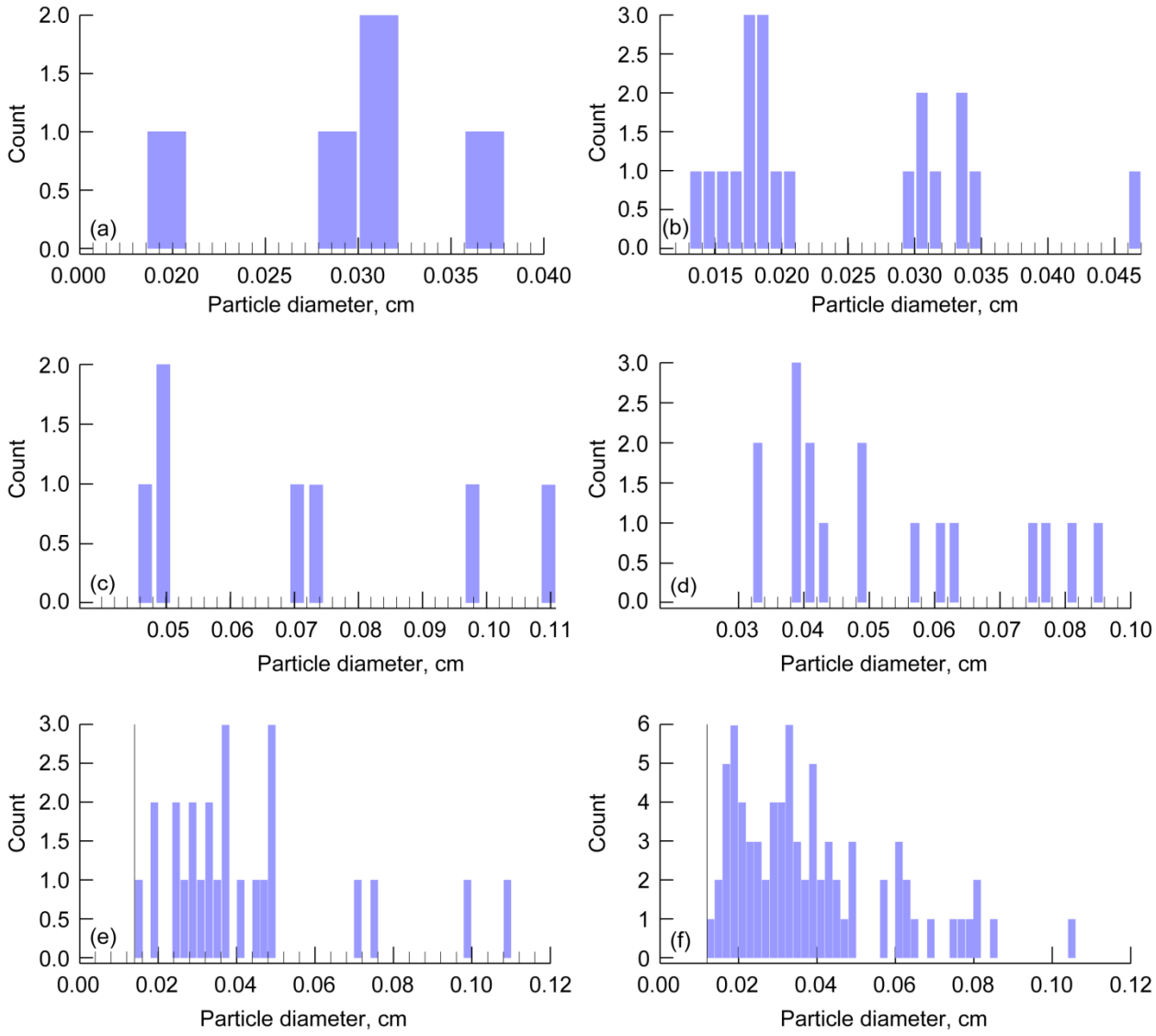

Figure 16.—Shows the fragmentation distribution from the crater data for the different projectiles used for impacting the unstressed and stressed titanium coupons that are shielded with an aluminum layer of ~0.04 in. in thickness. (a) d_p = 1.6 mm, V_p = 6.69 km/s, Al. (b) No.1985; d_p = 1.58 mm, V_p = 6.99 km/s, Al. (c) d_p = 3.6 mm, V_p = 6.87 km/s, nylon. (d) No. 1989; d_p = 3.59 mm, V_p = 7 km/s, nylon. (e) and (f) All fragments from all projectiles.

TABLE 3.—EXPERIMENTAL RESULTS OF THE RESIDUAL STRENGTH MEASUREMENTS
[The row labelled "Reference" corresponds to measurements of un-impacted titanium.]

Plate Identification	*Young's Modulus E (Msi)*	*0.2 Yield Strength S_y (ksi)*	*Ultimate Strength S_u (ksi)*	*Fracture Stress S_f (ksi)*	*Elongation E_f (%)*	*Area Reduction RA(%)*
Reference	17.2	144	151	123	15	34
8606	17.5	144	153	148	11	14
8373	17.3	145	152	139	13	24
8374	17.5	145	153	136	14	26
8375	17.3	144	152	134	15	29
8376	17.3	144	152	149	11	14
8377	17.1	144	148	146	5	8

Very little difference in Young's modulus, yield strength, and ultimate strength are exhibited, however, significant differences occur for the fracture strength, elongation and area reduction. The lower fracture strength and ductility are a result of the MMOD causing localized yielding and premature failure as compared to a smooth section. The large ductility and fracture toughness of Ti-6-4 allowed load shedding and good ultimate strength. Although the tensile results indicate little change in some engineering tensile values, the local strain are substantially higher in some cases as shown in Figure 17.

The localized strains at net section yield are about 30 percent higher, and at failure they are more than 3 times higher. Thus it was concerning that the quasi-static tensile tests do not represent well the localized damage, and it might be expected that components subjected load-control failure scenarios, such as pressure vessels, could fail at lower section stresses over time, as load cannot be easily redistributed. To investigate this point further, a specimen with a 0.11 by 0.32 by 0.33 mm crater was held under a constant load of 110 ksi stress for 21 hr. The results showed a constant strain under this condition as depicted in Figure 18. The concern is alleviated by the fact that the pressure is low compared to the usual high pressure common to pressure vessels and by Figure 18 which shows no strain increase under constant load over a period of 21 hr.

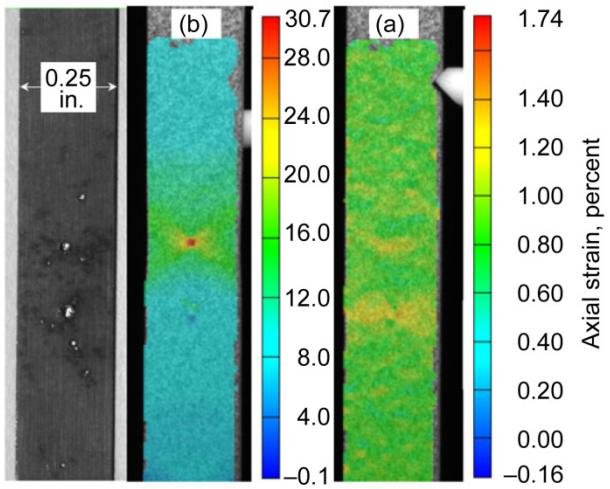

Figure 17.—Localized strain field near a crater at yield and prior to specimen fracture. Note the extreme increase in strain at the crater location.

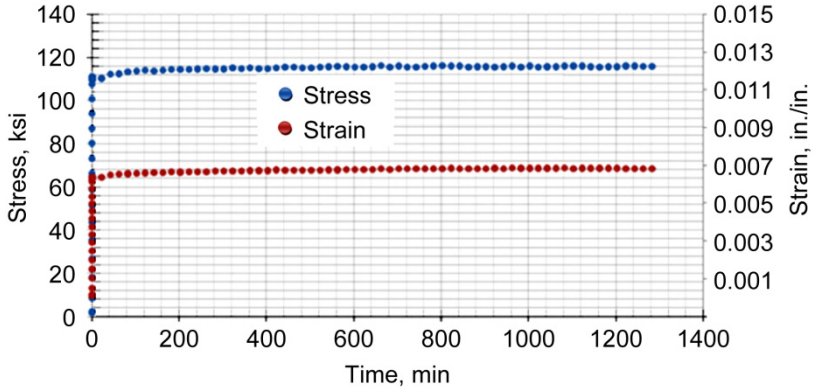

Figure 18.— Stress and the strain of a specimen with one small crater of ~10 percent penetration of the Ti thickness. The strain is shown to remain constant after 21 hr of constant loading at 110 ksi.

Concluding Remarks

In this paper, we showed the results of a series of hypervelocity impact tests in which a projectile is launched at an aluminum bumper in front of a titanium plate in order to understand the structure of the craters on the titanium caused by the projectile-bumper interaction and the resulting plume composed of projectile remains and target fragments. Several post impact tests performed on the titanium craters showed that the damage structures on the biaxially stressed and unstressed titanium plates were similar. Hardness measurements showed no differences between the Ti hardness under the crater and aside from the crater. This suggests that the local deformation upon impact does not affect the hardness properties even for the deepest crater of 38 percent depth analyzed in this work. Post impact residual strength measurements showed no discernable differences in the engineering strength properties between the pristine and cratered titanium. However, imaging of the strain field revealed significant increase in the localized strains upon tensile yield of the specimen. These measurements also revealed reduction in the fracture strength and reduction in ductility of the cratered titanium specimens. Tensile stress of 110 ksi applied to a cratered specimen showed no changes in the strain for 21 hr duration which suggests that the constant load conditions at the operating stress of about 100 ksi is not a concern.

We recommend performing burst pressure tests on cratered coupons. These tests are based on pressurizing the back surface of a cratered titanium coupon and increasing the pressure until failure. Such a test would be more representative of the load control failure than quasi-static tensile tests. We also recommend performing strain field measurements on craters of depth between 10 to 30 percent under loading conditions and comparing the strain fields, the elongation, area reduction and fracture strength for the two craters. This will help determine the appropriate allowable penetration depth on the surfaces of the metallic titanium pressure vessel.

References

1. Cour-Palais BG., “Meteoroid protection by multiwall structures,” AIAA 69-372, 1969.
2. Christiansen, E., “Meteoroids/Debris Shielding,” TP 2003-210788, 2003.
3. ASTM E8 / E8M - 08 Standard Test Methods for Tension Testing of Metallic Materials.

REPORT DOCUMENTATION PAGE		Form Approved OMB No. 0704-0188

1. REPORT DATE *(DD-MM-YYYY)*	2. REPORT TYPE	3. DATES COVERED *(From - To)*
01-10-2010	Technical Memorandum	

4. TITLE AND SUBTITLE
Hypervelocity Impact of Unstressed and Stressed Titanium in a Whipple Configuration in Support of the Orion Crew Exploration Vehicle Service Module Propellant Tanks

5a. CONTRACT NUMBER

5b. GRANT NUMBER

5c. PROGRAM ELEMENT NUMBER

6. AUTHOR(S)
Nahra, Henry, K.; Christiansen, Eric; Piekutowski, Andrew; Lyons, Frankel; Keddy, Christopher; Salem, Jonathan; Miller, Joshua; Bohl, William; Poormon, Kevin; Greene, Nathanael; Rodriguez, Karen

5d. PROJECT NUMBER

5e. TASK NUMBER

5f. WORK UNIT NUMBER
WBS 644423.06.32.01.03

7. PERFORMING ORGANIZATION NAME(S) AND ADDRESS(ES)
National Aeronautics and Space Administration
John H. Glenn Research Center at Lewis Field
Cleveland, Ohio 44135-3191

8. PERFORMING ORGANIZATION REPORT NUMBER
E-17435

9. SPONSORING/MONITORING AGENCY NAME(S) AND ADDRESS(ES)
National Aeronautics and Space Administration
Washington, DC 20546-0001

10. SPONSORING/MONITOR'S ACRONYM(S)
NASA

11. SPONSORING/MONITORING REPORT NUMBER
NASA/TM-2010-216804

12. DISTRIBUTION/AVAILABILITY STATEMENT
Unclassified-Unlimited
Subject Categories: 88 and 26
Available electronically at http://gltrs.grc.nasa.gov
This publication is available from the NASA Center for AeroSpace Information, 443-757-5802

13. SUPPLEMENTARY NOTES

14. ABSTRACT
Hypervelocity impacts were performed on six unstressed and six stressed titanium coupons with aluminium shielding in order to assess the effects of the partial penetration damage on the post impact micromechanical properties of titanium and on the residual strength after impact. This work is performed in support of the definition of the penetration criteria of the propellant tanks' surfaces for the service module of the crew exploration vehicle where such a criterion is based on testing and analyses rather than on historical precedence. The objective of this work is to assess the effects of applied biaxial stress on the damage dynamics and morphology. The crater statistics revealed minute differences between stressed and unstressed coupon damage. The post impact residual stress analyses showed that the titanium strength properties were generally unchanged for the unstressed coupons when compared with undamaged titanium. However, high localized strains were shown near the craters during the tensile tests.

15. SUBJECT TERMS
Hypervelocity impacts; Shielding; Micrometeoroids and orbital debris; Craters; Micromechanical properties; Strain; Hardness

16. SECURITY CLASSIFICATION OF:			17. LIMITATION OF ABSTRACT	18. NUMBER OF PAGES	19a. NAME OF RESPONSIBLE PERSON
a. REPORT	b. ABSTRACT	c. THIS PAGE			STI Help Desk (email:help@sti.nasa.gov)
U	U	U	UU	19	19b. TELEPHONE NUMBER *(include area code)* 443-757-5802